Silicon-based optoelectronic integrated circuit for label-free bio/chemical sensor

Junfeng Song,[1,2,*] Xianshu Luo,[1] Jack Sheng Kee,[1] Kyungsup Han,[1,3] Chao Li,[1] Mi Kyoung Park,[1] Xiaoguang Tu,[1] Huijuan Zhang,[1] Qing Fang,[1] Lianxi Jia,[1] Yong-Jin Yoon,[3] Tsung-Yang Liow,[1] Mingbin Yu,[1] and Guo-Qiang Lo[1]

[1]*Institute of Microelectronics, A*STAR (Agency for Science, Technology and Research), 11 Science Park Road, Science Park II, 117685 Singapore*

[2]*State Key Laboratory on Integrated opto-electronics, College of Electronic Science and Engineering, Jilin University, Changchun, 130012 China*

[3]*School of Mechanical & Aerospace Engineering, Nanyang Technological University, 50 Nanyang Avenue, 639789 Singapore*

[*]*songjf@ime.a-star.edu.sg*

Abstract: We demonstrate a silicon-based optoelectronic integrated circuit (OEIC) for label-free bio/chemical sensing application. Such on-chip OEIC sensor system consists of optical grating couplers for vertical light coupling into silicon waveguides, a thermal-tunable microring as a tunable filter, an exposed microring as an optical label-free sensor, and a Ge photodetector for a direct electrical readout. Different from the conventional wavelength-scanning method, we adopt low-cost broadband ASE light source, together with the on-chip tunable filter to generate sliced light source. The effective refractive index change of the sensing microring induced by the sensing target is traced by scanning the supplied electrical power applied onto the tracing microring, and the detected electrical signal is read out by the Ge photodetector. For bulk refractive index sensing, we demonstrate using such OEIC sensing system with a sensitivity of ~15 mW/RIU and a detection limit of 3.9 μ-RIU, while for surface sensing of biotin-streptavidin, we obtain a surface mass sensitivity of S_m = ~192 μW/ng·mm^{-2} and a surface detection limit of 0.3 pg/mm^2. The presented OEIC sensing system is suitable for point-of-care applications.

OCIS codes: (250.3140) Integrated optoelectronic circuits; (280.1415) Biological sensing and sensors; (130.0250) Optoelectronics; (280.4788) Optical sensing and sensors; (130.3120) Integrated optics devices; (130.2790) Guided waves; (040.5160) Photodetectors; (220.4000) Microstructure fabrication; (230.3990) Micro-optical devices.

References and links

1. S. Mukhrji and N. Punjabi, "Label-free integrated optical biosensors for multiplexed analysis," J. Indian Inst. Sci. **92**, 254–293 (2012).
2. M. Cooper, *Label-free biosensors: Techniques and applications* (Cambridge, U.K.: Cambridge University, 2009).
3. J. S. Daniels and N. Pourmand, "Label-free impedance biosensors: opportunities and challenges," Electroanalysis **19**(12), 1239–1257 (2007).
4. X. Fan, I. M. White, S. I. Shopova, H. Zhu, J. D. Suter, and Y. Sun, "Sensitive optical biosensors for unlabeled targets: A review," Anal. Chim. Acta **620**(1-2), 8–26 (2008).
5. F. Vollmer and S. Arnold, "Whispering-gallery-mode biosensing: label-free detection down to single molecules," Nat. Methods **5**(7), 591–596 (2008).
6. K. De Vos, I. Bartolozzi, E. Schacht, P. Bienstman, and R. Baets, "Silicon-on-insulator microring resonator for sensitive and label-free biosensing," Opt. Express **15**(12), 7610–7615 (2007).
7. K. De Vos, J. Girones, S. Popelka, E. Schacht, R. Baets, and P. Bienstman, "SOI optical microring resonator with poly(ethylene glycol) polymer brush for label-free biosensor applications," Biosens. Bioelectron. **24**(8), 2528–2533 (2009).

#186886 - $15.00 USD Received 12 Mar 2013; revised 25 Apr 2013; accepted 29 Apr 2013; published 19 Jul 2013

8. D.-X. Xu, M. Vachon, A. Densmore, R. Ma, A. Delâge, S. Janz, J. Lapointe, Y. Li, G. Lopinski, D. Zhang, Q. Y. Liu, P. Cheben, and J. H. Schmid, "Label-free biosensor array based on silicon-on-insulator ring resonators addressed using a WDM approach," Opt. Lett. **35**(16), 2771–2773 (2010).
9. M. Iqbal, M. A. Gleeson, B. Spaugh, F. Tybor, W. G. Gunn, M. Hochberg, T. Baehr-Jones, R. C. Bailey, and L. C. Gunn, "Label-free biosensor arrays based on silicon ring resonators and high-speed optical scanning instrumentation," IEEE J. Sel. Top. Quantum Electron. **16**(3), 654–661 (2010).
10. S. Janz, D.-X. Xu, M. Vachon, N. Sabourin, P. Cheben, H. McIntosh, H. Ding, S. Wang, J. H. Schmid, A. Delâge, J. Lapointe, A. Densmore, R. Ma, W. Sinclair, S. M. Logan, R. Mackenzie, Q. Y. Liu, D. Zhang, G. Lopinski, O. Mozenson, M. Gilmour, and H. Tabor, "Photonic wire biosensor microarray chip and instrumentation with application to serotyping of *Escherichia coli* isolates," Opt. Express **21**(4), 4623–4637 (2013).
11. J. Song, X. Luo, X. Tu, M. K. Park, J. S. Kee, H. Zhang, M. Yu, G.-Q. Lo, and D.-L. Kwong, "Electrical tracing-assisted dual-microring label-free optical bio/chemical sensors," Opt. Express **20**(4), 4189–4197 (2012).
12. K. W. Kim, J. Song, J. S. Kee, Q. Liu, G.-Q. Lo, and M. K. Park, "Label-free biosensor based on an electrical tracing-assisted silicon microring resonator with a low-cost broadband source," Biosens. Bioelectron. **46**, 15–21 (2013).
13. D. C. Duffy, J. C. McDonald, O. J. A. Schueller, and G. M. Whitesides, "Rapid Prototyping of Microfluidic Systems in Poly(dimethylsiloxane)," Anal. Chem. **70**(23), 4974–4984 (1998).
14. Q. Fang, J. Song, X. Luo, L. Jia, M. Yu, G. Lo, and Y. Liu, "High efficiency ring-resonator filter with NiSi heater," IEEE Photon. Technol. Lett. **24**(5), 350–352 (2012).
15. X. Tu, J. Song, T.-Y. Liow, M. K. Park, J. Q. Yiying, J. S. Kee, M. B. Yu, and G.-Q. Lo, "Thermal independent Silicon-Nitride slot waveguide biosensor with high sensitivity," Opt. Express **20**(3), 2640–2648 (2012).
16. H. Gu, Z. Ng, T. C. Deivaraj, X. Su, and K. P. Loh, "Surface plasmon resonance spectroscopy and electrochemistry study of 4-nitro-1,2-phenylenediamine: A switchable redox polymer with nitro functional groups," Langmuir **22**(8), 3929–3935 (2006).

1. Introduction

Label-free optical bio/chemical sensor is widely used to detect the refractive index change of bio/chemical targets, which is with numerous advantages, such as non-physical contact, high stability, high-speed detection, and high resolution etc. It is essential for the applications of medical diagnosis, healthcare, and environmental monitoring [1–4]. Various kinds of optical bio/chemical sensors are proposed and demonstrated, including surface-plasma resonance-based devices, optical interferometers, optical fiber devices, grating-based devices, photonic crystal structures, and micro-resonators devices [4–6]. Among all the approaches, silicon-on-insulator (SOI) based bio/chemical sensors have been attracting great research interests due to the advantage of large refractive index contrast, which enables the compact device footprint. Furthermore, the fabrication of SOI-based devices is CMOS compatible, which enables large-scale optoelectronic integrated circuits (OEIC). Plenty of SOI-based optical bio/chemical sensors have been demonstrated with the detection limit as low as 10^{-5}~10^{-7} [6–9]. A large number multiple channel microring sensor integration system is also demonstrated recently [10].

In general, there are two basic methods for optical sensing, namely, intensity scanning method and wavelength scanning method [9]. As the sensitivity of the intensity scanning method largely depends on the probe wavelength and the sensitivity of the photodetector in order to achieve high signal-to-noise ratio to maximize the intensity change, most of the demonstrated microresonator-based sensors adopt the wavelength-scanning method for measuring the sharp resonance wavelength shift. However, the wavelength-scanning method requires expensive high-resolution wavelength-tunable lasers, and thus the detection limit is ultimately limited by the laser resolution. Therefore, the high-resolution wavelength-scanning method might not be suitable for cost-effective point-of-care applications.

In order to overcome this aforementioned issue, we have proposed and demonstrated an electrical tracing-assisted dual-microring label-free optical bio/chemical sensor [11]. We integrated two cascade microrings on a single chip. One of microring is integrated with a heater for thermal tuning, named as tracing microring. The other microring serves as the sensing microring. The effective refractive index change of the detecting target is obtained by scanning the voltage that is supplied to the tracing microring by monitoring the output intensity from the sensing microring based on filter cascading effect. We demonstrated the

#186886 - $15.00 USD Received 12 Mar 2013; revised 25 Apr 2013; accepted 29 Apr 2013; published 19 Jul 2013

sensitivity of ~4.0 mW/ng·mm^{-2} and detection limit of ~5.35 pg/mm^2. Following this work, we integrated the one-dimensional grating coupler for the vertical light coupling between optical fiber and on-chip waveguides, which is suitable for practical application with device packaging [13]. However, such demonstrations still requires expensive off-the-shelf photodetector. Furthermore, the power consumption of the tracing microring, about ~20 mW, is relatively high.

In this paper, we demonstrate silicon-based OEIC for optical bio/chemical sensor by integrating grating couplers, a tunable microring filter, a microring sensor, and a Ge photodetector in a single chip. With the integrated Ge photodetector, we directly read out the electrical signal and extract the effective refractive index change. Furthermore, we adopt the undercut technique and remove the substrate Si, thus reduce tracing microring power consumption to be less than 3 mW. The demonstrated sensing sensitivity is ~15 mW/RIU and the detection limit is ~3.9 μ-RIU. For surface sensing, we obtain a surface mass sensitivity of S_m = ~192 μW/ng·mm^{-2} and the detection limit of 0.3 pg/mm^2. Such high-performance OEIC sensing system is with low-cost and promising for the potential large-scale integration, hence being suitable for point-of-care applications.

2. Working principle

Conventionally, the microresonator-based optical bio/chemical sensors use wavelength-scanning method in order to obtain the resonance wavelength shift induced by the effective refractive index change, as schematically shown in Fig. 1(a). A high-resolution wavelength scanning laser is deployed as the light source. The off-the-shelve photodetector records the transmission spectra. The refractive index change is extracted by the resonance wavelength shift. In such a method, the detection limit is determined by the resolution of the wavelength-tunable laser and the sensitivity of the photodetector. In order to resolve small changes of the resonance wavelength shift to detect ultra-small refractive index change, very high-resolution wavelength-tunable laser and highly sensitive photodetector are required, which would increase the cost significantly.

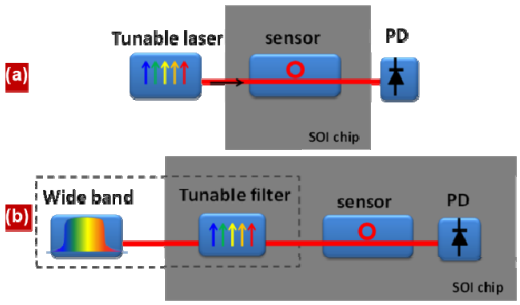

Fig. 1. (a) Schematic of the conventional wavelength-scanning method. (b) Schematic of the proposed silicon-based OEIC sensing system by using electrical-tracing-assisted sensing method.

In order to low-down the sensing cost, we propose an electrical tracing-assisted sensing method [11]. The basic idea is to combine a broadband light source witch limited free-spectral range (FSR) and a tunable filter as a tunable laser, which is indicated by the dashed box in Fig. 1(b). Furthermore, we integrate the tunable filter, the sensing microring, and the photodetector in a single silicon chip for lab-on-chip application.

Figure 2 shows the design schematic of the proposed optical sensing system. A broadband light source is vertically coupled into the silicon waveguide via a one dimensional (1D) grating coupler from a vertical optical fiber. Another merit of the vertical grating coupler is the polarization selectivity as only TE-polarized light is coupled into silicon chip, which avoids the disturbance from the TM-polarized light. A thermal-tunable microring resonator,

#186886 - $15.00 USD Received 12 Mar 2013; revised 25 Apr 2013; accepted 29 Apr 2013; published 19 Jul 2013

named as tracing microring, serves as the tunable filter [11]. Both tracing- and sensing-microring are Add/Drop microring resonator structure. The dropped light from microring resonator becomes a Lorentz-shaped narrow band. The centre wavelength is the microring resonance wavelength, and the linewidth of such dropped light is determined by the microring resonance quality factors (Q-factor). The higher the Q-factor is, the narrower the linewidth is. If both resonance wavelengths of the tracing- and sensing- microrings are aligned with each other, the output signal has the maximum intensity. By scanning the voltage supplied to the tracing microring to shift the resonance wavelength, both wavelengths are always aligned and the output intensity reaches maximum. By comparing the additional electrical power difference supplied to the tracing microring in order to trace the sensing microring wavelength change, the refractive index change is detected [11].

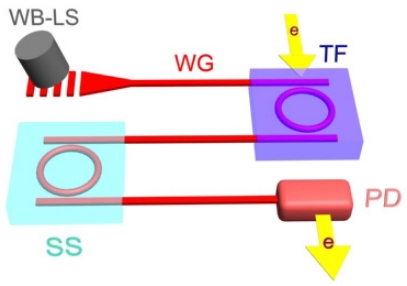

Fig. 2. Schematic of the proposed label-free optical bio/chemical sensing system. WB-LS: wideband light source. WG: waveguide; TF: tunable filter (tracing microring); SS: sensing microring; PD: photodetector.

3. Device fabrication

We fabricate the OEIC sensing system in silicon-on-insulator (SOI) platform by using CMOS-compatible fabrication processes. The SOI wafer has a 220 nm silicon layer sitting on a 2 μm buried oxide (BOX) layer. The device is patterned by using deep ultra-violet (DUV) photolithography, followed by two steps of silicon reactive ion etching (RIE) to form the vertical grating coupler and the slab waveguide with thickness of 150 nm, and the channel waveguide. We design the slab waveguide for light propagating, while adopt channel waveguides for the microring waveguides in order to minimize the optical transmission loss and meanwhile keep high sensitivity of sensing microring. For the Ge photodetector, separate masks are used for boron implantation to form the P type silicon under Ge, and P^+ type silicon Ohmic contacts. The implants are activated using rapid thermal anneal of 1050 °C for 5 seconds. After depositing a thin layer of field oxide, Ge epitaxial windows are opened by a combination of dry and wet etching to expose the underlying Si. After growing a thin SiGe buffer layer at 350 °C, Ge is selectively grown in an ultrahigh vacuum chemical vapor deposition (UHVCVD) epitaxial reactor at 550 °C with a thickness of 500 nm. The N^+ Ohmic contact is formed by implanting phosphorus into Ge top surface, followed by an annealing at 500 °C for 5 min. A layer of SiO_2 is deposited and the wafer goes through chemical-mechanical polish (CMP) with1 μm-thick oxide insulating layer remained. The purpose of CMP is reducing the surface step height. Following the deposition and patterning of TiN for the thermal heater, another 500 nm insulating oxide deposition, separate contact holes to the Si and Ge implantation regions and the thermal heater are opened by dry etching process, followed with 0.75 μm Al metal deposition and patterning for the electrical pad. A planarization step is carried out by depositing 1 μm oxide, reverse pattering/etching, and CMP again for the microfluidic channel packaging. The sensing windows and bond pad windows are opened afterwards via a combination of RIE dry etch and wet etch. Poly (dimethysiloxane) (PDMS) microfluidic channels are separately fabricated using a standard PDMS molding process [16]. A PDMS fluidic channel was bonded onto the diced silicon

#186886 - $15.00 USD Received 12 Mar 2013; revised 25 Apr 2013; accepted 29 Apr 2013; published 19 Jul 2013

sensor chip via activation of the silicon surface as well as the PDMS surface using the oxygen plasma.

Figures 3(a)-3(d) show the scanning electrode microscopes (SEMs) of the building blocks of the sensing system, including the vertical grating coupler in Fig. 3(a), the thermal tunable tracing microring in Fig. 3(b), the sensing microring in Fig. 3(c), and the Ge photodetector in Fig. 3(d). The grating period is designed as 630 nm with a filing factor 50%. The etch depth of the grating coupler is 70 nm. We adopt a low power consumption thermal tunable tracing microring by using isolation trenches. The silicon substrate of the microring resonator is etched away in order to efficiently confine the generated thermal heating, thus lower down the electrical power consumption significantly [14]. Both tracing microring and sensing microring are designed identically with 10 μm radius and 20 μm interaction lengths with a gap of 300 nm between waveguide and microring. The on-chip Ge photodetector is designed with 6 μm width and 100 μm length, which is sufficient for the light absorption.

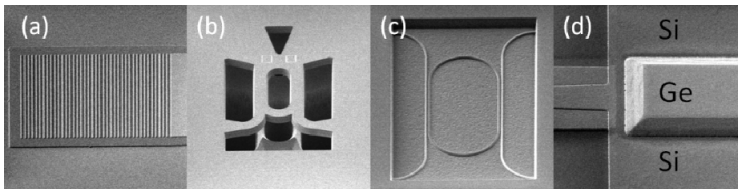

Fig. 3. The SEMs of the building blocks. (a) Optical one dimensional grating coupler. (b) Thermal-optical tunable ring filter. (c) Sensing microring. (d) Ge photodetector.

4. Device characterization and results discussion

4.1 Testing setup

Figure 4(a) shows the schematic of the testing setup. We use a broadband ASE as the light source. An external tunable bandpass filter is used in order to limit the input light source to one free-spectral range (FSR). The light is coupled into the silicon waveguide via the grating coupler. A semiconductor device analyzer (SDA) is adopted to supply the power to the tracing microring and also collect the generated photocurrent from the Ge photodetector. Figure 4(b) shows the optical image of the packaged sensing system, including the bonded electrical wires on PCB board, the microfluidic pipeline, and the input/output vertical coupling fibers.

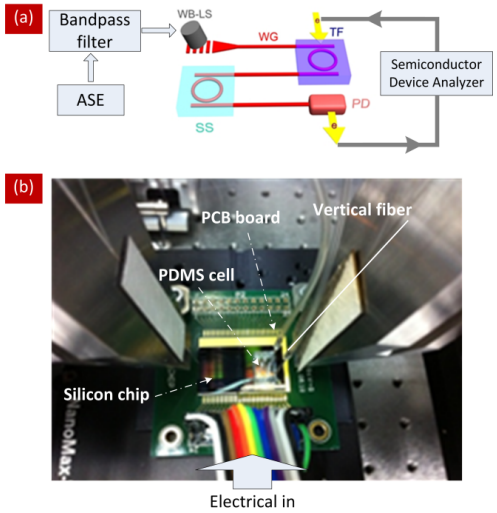

Fig. 4. (a) Schematic of the testing setup. (b) The optical image of the biochip on the test setup.

#186886 - $15.00 USD Received 12 Mar 2013; revised 25 Apr 2013; accepted 29 Apr 2013; published 19 Jul 2013

4.2 Characterization of the tracing microring with isolation trench

The resonance wavelength λ_r of the microring resonator (both tracing- and sensing-microrings) depends on the waveguide effective refractive index n_{eff}, which is determined by the environment situations, including the temperature T for the tracing microring, and optical index n_c of the cladding material (sensing target) on the sensing microring. The relationship among them can be expressed as:

$$\Delta\lambda_r = \frac{\lambda_r}{n_g}\left(\frac{\partial n_{eff}}{\partial T}\Delta T + \frac{\partial n_{eff}}{\partial n_c}\Delta n_c\right) \quad (1)$$

where, n_g is the group index of waveguide, ΔT and Δn_c are temperature change and the index change of the target objective (sensing microring cladding index change).

Firstly, we characterized a stand-alone tracing microring (the tunable filter), which is fabricated in the same chip with identical designs of the sensing microring. In the tracing microring, $\Delta n_c = 0$, while the temperature change ΔT linearly relates to the heater power variation of ΔW. In such case, we link the resonance wavelength shift to the electrical power change as:

$$\Delta\lambda_r = A\Delta W \quad (2)$$

where, coefficient A is the *sensitivity* of the tracing microring to electrical power. Figure 5(a) shows the measured transmission spectra of the tracing microring upon different voltages. The voltage increases from 0 V to 1.2 V with a step of 0.2 V. As the supplied voltage increases, the microring effective refractive index increases due to the increase of the temperature. The measured resistivity of the thermal heater R is ~940 Ω. Thus, the relation between the resonance wavelength to the electrical power is calculated with $W = V^2/R$ and is shown in Fig. 5(b). The extracted thermal coefficient is ~3.4 nm/mW. However, for the identically designed tunable microring without isolation trench, the thermal coefficient is only ~0.155 nm/mW, suggesting a 20 times enhancement. As the FSR of the microring is ~5.5 nm, the resonance shift of an FSR requires 1.62 mW electrical powers, which corresponds to the voltage supply of ~1.23 V.

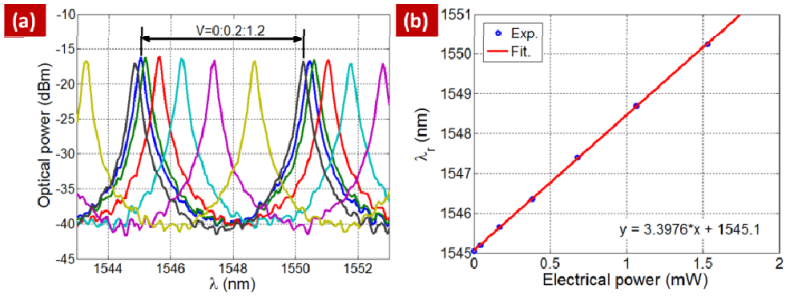

Fig. 5. (a) The measured transmission spectra of the tracing microring upon different electrical voltages. Voltage increases from 0 V to 1.2 V with step of 0.2V. (b) The resonance wavelength as function of the electrical power supplying to the tracing microring. Blue circles are experimental data from (a) and red line is linear fitting curve.

4.3 Characterization of the microring sensor

We then characterize the performance of the identically designed stand-alone microring sensor. In the sensing microring, the temperature variation is ignored, as the tracing microring and sensing microring are separated far enough to avoid the thermal interaction. Thus, the resonance wavelength variation depends on only the cladding index variation linearly, as indicated in Eq. (1).

#186886 - $15.00 USD Received 12 Mar 2013; revised 25 Apr 2013; accepted 29 Apr 2013; published 19 Jul 2013

$$\Delta\lambda_r = S\Delta n_c \tag{3}$$

Where, S is the sensitivity of the sensing microring to the target objective. Furthermore, the sensing sensitivity can be expressed as:

$$S = \frac{\lambda_r}{n_g}\frac{\delta n_{eff}}{\delta n_c} \tag{4}$$

Where, $\delta n_{eff}/\delta n_c$ is determined by light distribution in the waveguide and in the cladding. The weaker the light confinement inside the waveguide is, the stronger the light interaction with the cladding material, the larger the value of $\delta n_{eff}/\delta n_c$. n_g is the group index and is dependent on the dispersion of waveguide materials and waveguide dimension. In our design, n_g is ~4.2.

In order to experimentally investigate the sensing sensitivity, we employ NaCl solution as the detecting target. The concentrations of the NaCl solution used are 1%, 3%, 5%, 7% and 10%. The relation between concentration and the index is as $n = 0.17151C + 1.3119$, where C is the concentration. Figure 6 shows the measured resonance wavelength as function of the refractive index of the NaCl solution. The extracted sensing sensitivity is ~58.3 nm/RIU.

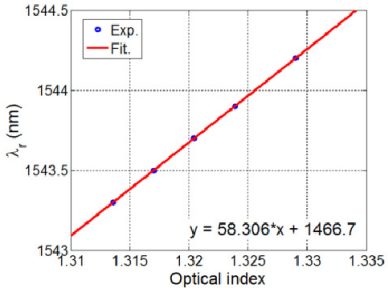

Fig. 6. The resonance wavelength shift of the sensing microring with different concentration of the cladding NaCl solutions. Five different concentrations are adopted as 1%, 3%, 5%, 7% and 10%, respectively.

4.4 Characterization of the Ge photodetector

Figure 7 shows the photodetector current-voltage (I-V) curves with (red line, on) and without (blue line, off) light illumination. The I-V curves are measured by aligning both resonances together in order to maximize the optical power reaching to the Ge PD. We also compare the current enhancement upon different bias voltage supply with and without light illumination, as shown in Fig. 7(b). It suggests that at 0 V bias, the current enhancement is as large as 62 times of that with light illumination. Thus, in the following measurement, we operate the Ge photodetector with 0 V voltage bias.

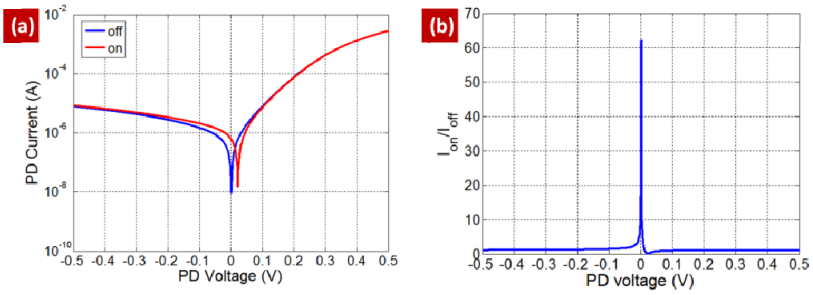

Fig. 7. (a) The measured I-V curve of the Ge-Photodetector with (red) and without (blue) light illumination. (b) The enhancement of the photocurrent with and without light illumination.

#186886 - $15.00 USD Received 12 Mar 2013; revised 25 Apr 2013; accepted 29 Apr 2013; published 19 Jul 2013

4.5 Demonstration of optical sensing using OEIC sensing system

We then demonstrate the optical bio/chemical sensing using such OEIC sensing system including the detection of the bulky refractive index change and the surface sensing of specific protein.

For bulk refractive index sensing, we characterize the detection limit of the sensing system by using NaCl solution as the detection target. For the sensing microring upon different concentrations of the NaCl solution, we scan the applied voltage to the tracing microring and record the photocurrent generated from the on-chip photodetector. Figure 8(a) shows the measured photocurrent spectra upon the scanning of the electrical power to the tracing microring. By using Lorentz fitting [11], we obtain the required electrical power at which the peak current achieved, and subsequently relate that to the index change of the NaCl solution upon different concentrations. Figure 8(b) shows the extracted relationship between the optical refractive index of the NaCl solution and the electrical power supplied to the tracing microring. The sensing sensitivity according to linear fitting is ~15 mW/ RIU.

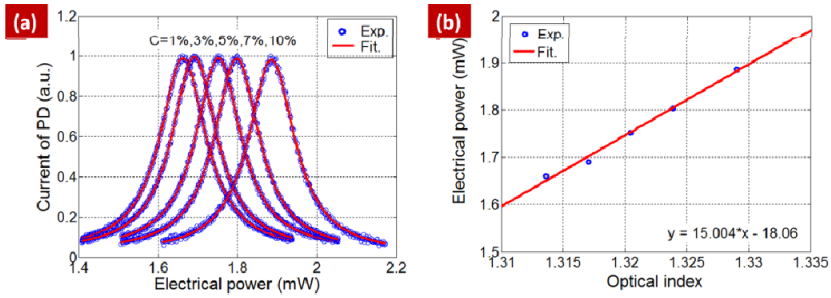

Fig. 8. (a) The measured photocurrent spectra upon the scanning of the electrical power to the tracing microring with different NaCl concentrations. The blue circle lines are the experimental measurements while the red lines are the fitting results. (b) The relationship between the extracted electrical power and the optical index of the NaCl solutions.

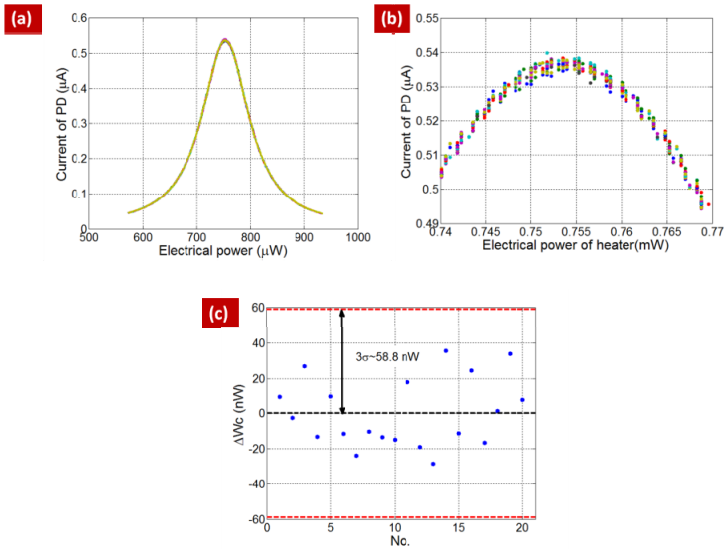

Fig. 9. (a) The measured photocurrent spectra upon the supplied electrical power to the tracing microring. There are 20 times repeat measurements. (b) Zoom in of (a) around spectra peeks. (c) The electrical power deviation for 20 measurements. σ: standard deviation, 3σ: the extracted electrical power resolution.

#186886 - $15.00 USD Received 12 Mar 2013; revised 25 Apr 2013; accepted 29 Apr 2013; published 19 Jul 2013

From Eqs. (2) and (3), the detection limit relates to the electrical power resolution, which can be determined by measuring the standard deviation of the supplied electrical power. This is obtained by repeating the measurement for multiple times. Figure 9(a) shows as an example the photocurrent spectra as function of the electrical power with 20 times measurement. The voltage is scanned at a step of 0.5 mV and sensing microring is exposed to the air. The zoom-in views of the intensity distributions around peak intensity are shown in Fig. 9(b). The peak positions of every measurement can be extracted by Lorentz fitting to the optical response [11]. The obtained electrical powers corresponding to the peak current are shown in Fig. 9(c). The extracted standard deviation σ is ~19.6 nW, suggesting the electrical power resolution 3σ of 58.8 nW. Such high resolution can be attributed to the following reasons: 1) the electrical tracing assisted sensing method is intrinsically with high resolution comparing to the wavelength-scanning method due to the achievable smaller equipment resolution [11]. For instance, the equivalent wavelength resolution is calculated to be ~0.2 pm in current demonstration. 2) the data fitting adopted here smooth the measurement results, thus enhancing the signal-to-noise ratio, and 3) the measurement for achieving the standard deviation is with air cladding in order to make sure the stable testing system. This may introduce slight difference comparing to the sensing microring that cladded with detection objective. Based on the extracted detection resolution, the detection limit is ~3.9 μ-RIU.

For surface sensing of specific protein interaction, a well-characterized biotin-streptavidin interaction is used as a model system. The interaction between biotin and streptavidin is one of the highest non-covalent affinities ($K_D = 10^{-13}$ M) and is therefore stable and specific. The silicon microring device is first treated with oxygen plasma during a PDMS bonding process. It is then treated by injecting a solution of 2% 3-aminopropyltriethoxysilane (APTES, Sigma-Aldrich) in a mixture of ethanol/H_2O (95%/5%, v/v) using a syringe pump for 2 h, followed by thorough rinsing with ethanol. It is then treated through injection of a solution of 0.25 mg/ml NHS-PEG_4-biotin (Thermo Scientific Pierce) in DI water for 1 h and rinsed with DI water in the same method. In addition, 1% bovine serum albumin (BSA, Sigma-Aldrich) in phosphate buffered saline (PBS) is injected into microchannel for 30 min to prevent non-specific binding at the surface of a silicon microring device and rinsed with PBS. The binding assay between biotin and streptavidin is performed by applying streptavidin solution in PBS.

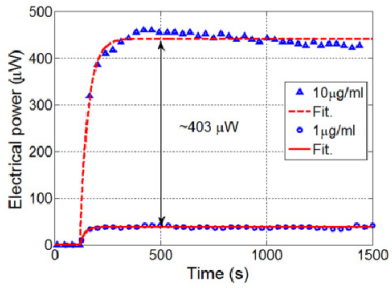

Fig. 10. Real time detection of biotin-streptavidin interaction. Blue triangles and circles are the experimental data of 10 μg/ml and 1 μg/ml, respectively. Red dashed line and solid line are the fitting results.

Figure 10 shows the supplied electrical power of the tracing microring with biotin-streptavidin interaction time. The blue triangle and circle markers are the supplied electrical power supplied in order to trace the effective index change of the sensing microring upon 10 μg/ml and 1 μg/ml solutions, respectively. Upon the exposure of the sensing microring to streptavidin solution, the electrical power rapidly increased, which indicates an increase in the effective index on the sensor surface resulting from the binding of streptavidin molecules to immobilized biotin on the sensor surface. The electrical power reached saturation after 5 min of binding. The electrical power increments from biotin/streptavidin interaction at the

#186886 - $15.00 USD Received 12 Mar 2013; revised 25 Apr 2013; accepted 29 Apr 2013; published 19 Jul 2013

saturation are ~38 μW and ~441 μW for 1 μg/ml and 10 μg/ml, respectively. Red-dashed line and solid line are the fitting results by using following equation:

$$W(t) = W_0 + (W_\infty - W_0)\left[1 - \exp\left(-\frac{t - t_0}{\tau}\right)\right] \quad (5)$$

where, $W(t)$ is the instantaneous electrical power, W_0 is the initial power, W_∞ is the final steady state power, t_0 is the start time of interaction, τ is the interaction time. For 10 μg/ml and 1 μg/ml, the interaction times τ are 32 seconds and 22 seconds, respectively. Considering the strong affinity between biotin and streptavidin, we assume that the sensor surface is saturated with streptavidin molecules at 10 μg/ml, resulting in ~441 μW increase in electrical power.

The sensitivity for surface binding detection is given by $S_m = \Delta W/\sigma_p$, where σ_p the surface density of streptavidin monolayer and ΔW is is the electrical power increase. With known surface coverage of streptavidin monolayer of 2.5×10^{10} molecules/mm^2 [16], the surface density is calculated to be ~2.3 ng/mm^2. Using the values of the electrical power increase from this experiment, we obtain a surface mass sensitivity of S_m = ~192 μW/ng·mm^{-2}. The detection limit of a sensor is defined by $L_m = R/S_m$, where R is the sensor resolution (3σ) and S_m is the mass sensitivity. If we consider 3σ of ~58.8 nW, we estimate the surface detection limit to be ~0.3 pg/mm^2.

5. Conclusion

We have fabricated a silicon-based OEIC for label-free optical bio/chemical sensor using CMOS-compatible fabrication process. Such OEIC sensing system integrates grating couplers, a tracing microring, a sensing microring, and a Ge photodetector on a single SOI chip, which features the advantage of large-scale integration and significantly reduced cost. By using electrical-tracing assisted sensing method, we have demonstrated the sensitivity of ~15 mW/RIU and the detection limit of 3.9 μ-RIU for bulky index sensing, and obtained a surface mass sensitivity of S_m = ~192 μW/ng·mm^{-2} and the detection limit of 0.3 pg/mm^2 for surface biotin-streptavidin sensing. Such OEIC sensing system is favored for point-of-care application with low electrical power consumption.

Acknowledgments

This work was supported by the Agency for Science, Technology and Research (A*STAR) Joint Council Office (JCO) Development Programme Grant (1234e00018), Singapore, and National Natural Science Foundation of China (NSFC, Grant No. 61177090).

#186886 - $15.00 USD Received 12 Mar 2013; revised 25 Apr 2013; accepted 29 Apr 2013; published 19 Jul 2013